photonic-crystal-based integrated circuits, as strong 3D confinement of photons in an ultra-small cavity has been realized, and leakage in the vertical direction sufficiently suppressed. □

Received 24 July; accepted 12 September 2003; doi:10.1038/nature02063.

1. Khitrova, G., Gibbs, H. M., Jahnke, F., Kira, M. & Koch, S. W. Nonlinear optics of normal-mode-coupling semiconductor microcavities. *Rev. Mod. Phys.* **71,** 1591–1639 (1999).
2. Noda, S., Chutinan, A. & Imada, M. Trapping and emission of photons by a single defect in a photonic bandgap structure. *Nature* **407,** 608–610 (2000).
3. Song, B. S., Noda, S. & Asano, T. Photonic devices based on in-plane hetero photonic crystals. *Science* **300,** 1537 (2003).
4. Painter, O. *et al.* Two-dimensional photonic band-gap defect mode laser. *Science* **284,** 1819–1821 (1999).
5. Noda, S., Tomoda, K., Yamamoto, N. & Chutinan, A. Full three-dimensional photonic bandgap crystals at near-infrared wavelengths. *Science* **289,** 604–606 (2000).
6. Spillane, S. M., Kippenberg, T. J. & Vahala, K. J. Ultralow-threshold Raman laser using a spherical dielectric microcavity. *Nature* **415,** 621–623 (2002).
7. Michler, P. *et al.* A quantum dot single-photon turnstile device. *Science* **290,** 2282–2285 (2000).
8. Johnson, S. G., Fan, S., Mekis, A. & Joannopoulos, J. D. Multipole-cancellation mechanism for high-*Q* cavities in the absence of a complete photonic band gap. *Appl. Phys. Lett.* **78,** 3388–3390 (2001).
9. Vučković, J., Lončar, M., Mabuchi, H. & Scherer, A. Design of photonic crystal microcavities for cavity QED. *Phys. Rev. E* **65,** 016608 (2001).
10. Srinivasan, K. & Painter, O. Momentum space design of high-*Q* photonic crystal optical cavities. *Opt. Express* **10,** 670–684 (2002).
11. Gayral, B. *et al.* High-*Q* wet-etched GaAs microdisks containing InAs quantum boxes. *Appl. Phys. Lett.* **75,** 1908–1910 (1999).
12. Yoshie, T., Vučković, J., Scherer, A., Chen, H. & Deppe, D. High quality two-dimensional photonic crystal slab cavities. *Appl. Phys. Lett.* **79,** 4289–4291 (2001).
13. Ryu, H. Y. *et al.* Square-lattice photonic band-gap single-cell laser operating in the lower-order whispering gallery mode. *Appl. Phys. Lett.* **80,** 3883–3885 (2002).
14. Armani, D. K., Kippenberg, T. J., Spillane, S. M. & Vahala, K. J. Ultra-high-*Q* toroid microcavity on a chip. *Nature* **421,** 925–928 (2003).
15. Vernooy, D. W., Ilchenko, V. S., Mabuchi, H., Streed, E. W. & Kimble, H. J. High-*Q* measurements of fused-silica microspheres in the near infrared. *Opt. Lett.* **23,** 247–249 (1998).
16. Yablonovitch, E. Inhibited spontaneous emission in solid-state physics and electronics. *Phys. Rev. Lett.* **58,** 2059–2062 (1987).
17. Akahane, Y., Asano, T., Song, B. S. & Noda, S. Investigation of high-*Q* channel drop filters using donor-type defects in two-dimensional photonic crystal slabs. *Appl. Phys. Lett.* **83,** 1512–1514 (2003).

Acknowledgements This work was supported partly by Grant-in-Aid from the Ministry of Education, Culture, Sports, Science and Technology of Japan, and also by CREST, Japan Science and Technology Corporation.

Competing interests statement The authors declare that they have no competing financial interests.

Correspondence and requests for materials should be addressed to S.N. (snoda@kuee.kyoto-u.ac.jp).

High interannual variability of sea ice thickness in the Arctic region

Seymour Laxon[1], **Neil Peacock**[1] **& Doug Smith**[2]

[1]*Centre for Polar Observation and Modelling, University College London, Gower Street, London WC1E 6BT, UK*
[2]*Met Office Hadley Centre for Climate Prediction and Research, FitzRoy Road, Exeter, Devon EX1 3PB, UK*

Possible future changes in Arctic sea ice cover and thickness, and consequent changes in the ice-albedo feedback, represent one of the largest uncertainties in the prediction of future temperature rise[1,2]. Knowledge of the natural variability of sea ice thickness is therefore critical for its representation in global climate models[3,4]. Numerical simulations suggest that Arctic ice thickness varies primarily on decadal timescales[3,5,6] owing to changes in wind and ocean stresses on the ice[7–10], but observations have been unable to provide a synoptic view of sea ice thickness, which is required to validate the model results[3,6,9]. Here we use an eight-year time-series of Arctic ice thickness, derived from satellite altimeter measurements of ice freeboard, to determine the mean thickness field and its variability from 65° N to 81.5° N. Our data reveal a high-frequency interannual variability in mean Arctic ice thickness that is dominated by changes in the amount of summer melt[11], rather than by changes in circulation. Our results suggest that a continued increase in melt season length would lead to further thinning of Arctic sea ice.

The prediction of future changes in Arctic sea ice, and consequent effects on the ocean[12] and atmosphere[2], relies on global climate models properly reproducing changes in ice thickness[3,4,13]. Knowledge of ice thickness variability is also critical in determining whether observed changes[14] are natural, or anthropogenic, in origin[4]. The sparseness of sea ice thickness observations means that current understanding of the regional, and interannual, variability of sea ice thickness is entirely based on numerical models of the Arctic[6,9]. However, it is unclear from model results whether ice thickness is controlled mainly by changes in thermodynamic (radiative or thermal) forcing[5], or by dynamic (ocean and wind stress) forcing[7]. The majority of Arctic Ocean models suggest that variability in Arctic ice thickness occurs on decadal timescales[5,6,9], and is caused mainly by dynamic forcing[6–8]. Simulations of Arctic ice cover covering the past four decades have been used to argue that observed thin ice[14–17] during the 1990s was a result of changes in atmospheric[6,7,10,17] or oceanic[8,18] circulation. However, numerical simulations of ice thickness are undermined by uncertainties in the representation of physical processes[9], and by differences in methods used to couple the ice, ocean and atmosphere[12], resulting in significant discrepancies between model simulations of ice thickness evolution[14]. The lack of continuous large-scale thickness measurements means that conclusions drawn from numerical simulations regarding the variability of Arctic sea ice thickness, and the processes that control it, remain untested[3,12].

We use newly developed techniques to obtain ice thickness from satellite estimates of ice freeboard over the 8-yr period 1993–2001 (Fig. 1). The region of coverage (ROC) extends to 81.5° N, covering an average area of 3.08×10^6 km^2, or more than half of the permanent sea ice cover. The data cover the entire circumference of the Arctic Ocean, including the Beaufort, Chukchi, East Siberian, Kara, Laptev, Barents and Greenland seas. We use measurements from the 13.8-GHz radar altimeters carried on the ERS-1 and ERS-2 satellites. By analysing individual echoes, we distinguish those originating from consolidated first and multi-year ice floes from those due to leads, open water and new ice. Corrections for orbits, tides, and atmospheric delay are applied to the radar data to obtain the elevation of ice floes and open water or new ice[19]. The elevation of the ice above the water surface is then obtained by subtracting the sea surface elevation, determined from open water measurements.

To deduce the ice thickness from ice elevation, the source of the echoes scattered from snow-covered sea ice must be determined. Laboratory experiments show that, under dry cold snow conditions, a normal-incidence 13.4-GHz radar reflection from snow-covered sea ice originates at the snow–ice interface[20]. The ERS radar altimeter measurements of ice elevation therefore provide the level of the snow–ice interface above the water level—that is, the ice freeboard. We convert the ice freeboard measurements to ice thickness by assuming hydrostatic equilibrium, and then using fixed densities of ice (915.1 kg m^{-3}) and sea water (1,023.9 kg m^{-3})[21] and a monthly climatology of snow depth and density[22]. The estimated uncertainty in ice and water density, of ± 5 kg m^{-3} and ± 0.5 kg m^{-3} respectively[21], results in an uncertainty of ± 11 cm for our mean thickness. Interannual variability in snow loading, estimated[23] to be between 2 and 3 cm, results in a further uncertainty of 6 to 9 cm in our ice thickness estimates. Figure 2 compares ERS thickness estimates with those derived from near-coincident submarine draught measurements[15]. A linear least-squares fit, weighted by the estimated measurement, snow loading and ice/water density uncertainties, shows that the correlation between the altimeter and

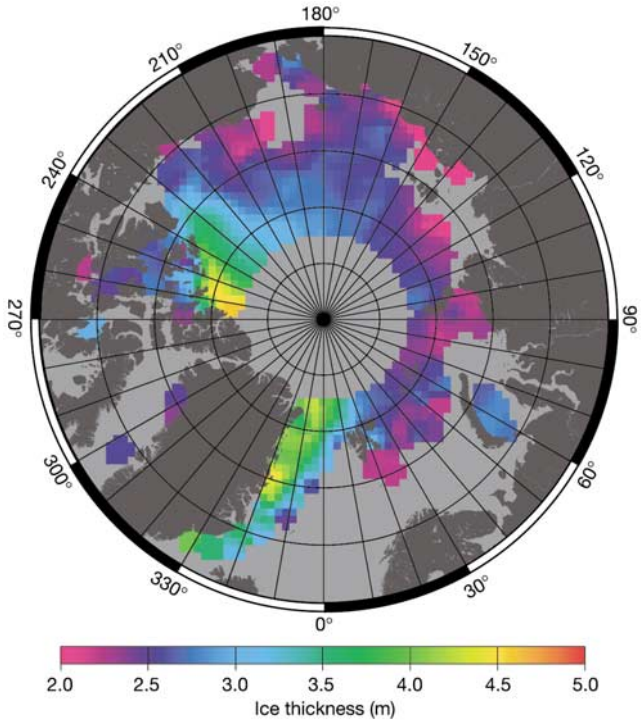

Figure 1 Average winter (October to March) Arctic sea ice thickness from October 1993 to March 2001 from satellite altimeter measurements of ice freeboard. Data are not available in the marginal ice zone, or above the ERS latitudinal limit of 81.5° N. Ice freeboard is converted to thickness using fixed ice, snow and water densities and regional monthly snow depth[22]. The mean thickness excludes thin ice (less than 0.5–1 m) and open water.

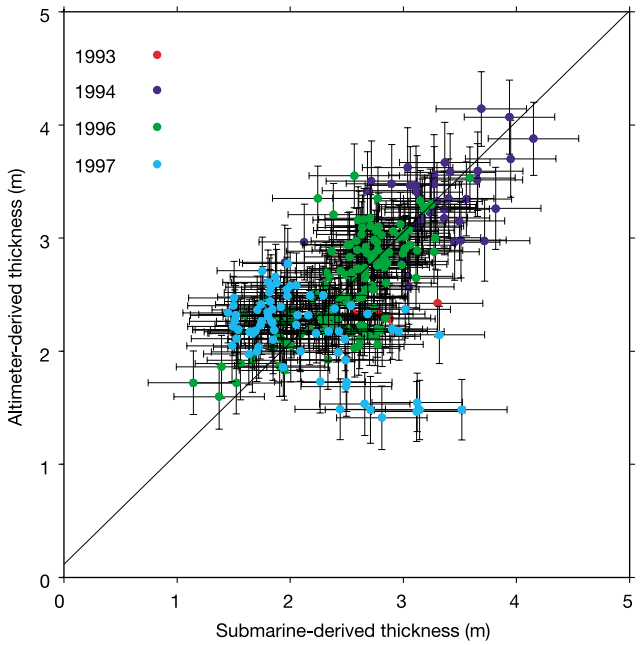

Figure 2 Comparison between satellite altimeter- and submarine-derived ice thickness in the Beaufort Sea during the 1990s. Submarine thicknesses are shown for each of the 50-km segments gathered during the four missions during the 1990s. Altimeter thickness estimates are generated from observations within 15 days and 100 km of the submarine draught sections. The submarine thicknesses exclude thin ice (<0.5 m) and open water, because (owing to difficulties in discriminating thin ice from open water) progressively more altimeter data are excluded once the ice thickness falls below 1 m. Error bars show uncertainties in altimeter thickness due to measurement errors and snow depth variability and an error in submarine thickness of 0.4 m, obtained by scaling the 0.3-m estimate of draught error[15] and adding the uncertainty in the snow depth used to convert to thickness. A linear least-squares fit (shown) yields a slope of 0.978 ± 0.082 and intercept 0.117 ± 0.207 m, with a χ^2 probability $Q = 0.999$. We do not account for the different spatial sampling of the two techniques, which may result in additional scatter between the two data sets.

submarine estimates is significant at the 99.9% level using a χ^2 goodness-of-fit test.

The altimeter thickness estimates exclude areas of thin ice (less than 0.5 to 1 m) and open water. Using submarine draught data, gathered during different years, we calculate that the fraction of thin ice and open water ranges from 20.0 ± 8.2% in September (4 cruises) and October (1 cruise), to 3.2 ± 1.4% in March (2 cruises) and early April (5 cruises). Published submarine analyses show that rapid thermodynamic growth of thinner ice reduces the fraction of thin ice and open water from 20% to 10% between September and October[24], and further to 3% by April[25]. Estimates from infrared satellite imagery show a reduction in thin ice fraction from 33% in September to 13% in October, and further to between 5 and 7% from January to April[26]. The estimates differ from those obtained from submarines owing to the lower accuracy of the infrared technique and because the infrared data are from only a single winter season. Taking the average of the submarine estimates of thin ice and open water fraction in October (10%) and March (3%), we estimate that the altimeter data exclude an average of 6.5% of the ice cover during winter. We calculate, using the submarine data, that the consequent bias in mean winter thickness is +18 cm. The standard deviation of the bias, due to the interannual variability of thin ice and open water, and to sampling differences between different submarine cruises, ranges from 15 cm in September and October, to 5 cm in March and April. We therefore estimate that the maximum contribution of the thin ice and open water to the standard deviation in mean winter ice thickness is 10 cm.

We obtain a mean winter ice thickness over the ROC (Fig. 1) of 2.73 m. The thickest ice is observed adjacent to the Canadian Archipelago and in the Fram Strait, as observed in previously published climatologies based on sparse submarine observations[27]. In the southern Beaufort Sea we observe an ice thickness of 2.5 m. This is thinner than the average submarine-observed draught of 3.7 m in 1976[27], but is consistent with field and submarine measurements during the 1990s[15,17]. No submarine climatology exists for the eastern sector of the ROC, but the average thickness that we find between 60° E and 150° E (2.4 m) lies within the range of sparse *in situ* thickness measurements made in the same region during the mid-1990s (1.8 to 2.8 m; ref. 28). The regional distribution of ice thickness that we obtain is, therefore, similar to submarine climatologies, but consistent with thinner ice in the Western Arctic during the 1990s[17].

We now examine the interannual variability in the average Arctic winter ice thickness over the ROC. We removed the mean thickness (Fig. 1) from individual measurements and, after applying a seasonal correction, averaged the residual thickness over each winter (October to March) to generate a time series of annual ice thickness anomalies (Fig. 3a). The average winter sea ice thickness over the ROC, excluding thin ice and open water, has a standard deviation of 24.5 cm, or 9% of the average, during the 8-yr period. This compares with a variability of 6% in ice mass in both Arctic[5] and global coupled climate models[3,29], over periods of 50 yr or more. The data show that the observed variability in ice mass is 50% greater than predicted by models, and probably more, as our measure excludes variability that occurs over timescales of longer than a

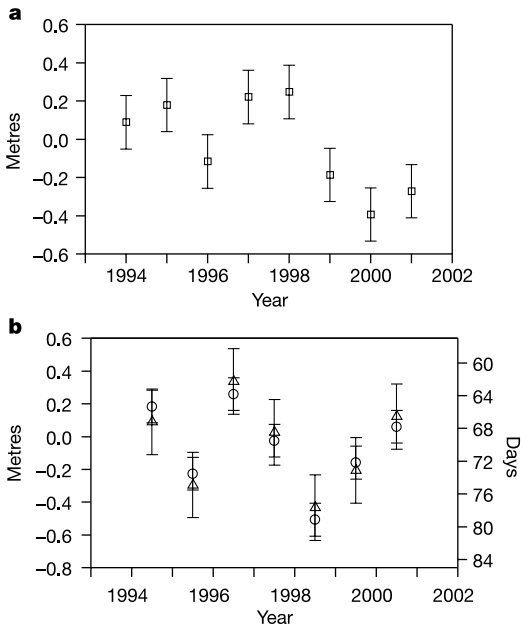

Figure 3 Time series of ice thickness anomalies and winter–winter change in thickness, compared with summer melt season length. **a**, Mean winter (October to March) ice thickness anomaly over the ROC for the period 1993–2001. The data show a spatial average of anomalies in ice thickness, obtained by subtracting the mean field (Fig. 1) from individual grids of average winter ice thickness. **b**, Changes in ice thickness between consecutive winters (circles) and melt season length (triangles) during the intervening summer period, derived from passive microwave observations[11]. The correlation between ice thickness change and melt season length is $R^2 = 0.926$, showing that, during the period of our observations, the variability of mean Arctic sea ice thickness was controlled almost entirely by changes in thermodynamic forcing.

decade. The interannual variability in thickness compares with a variability in mean annual ice extent of 1.7% during the same period. This undermines the conclusion, from numerical models[9], that changes in ice thickness occur on much longer timescales than changes in ice extent. The high-frequency variability shows that trends in ice thickness derived over periods of less than a decade[15], or from a single pair of submarine cruises[16], are susceptible to undersampling of the interannual variability in ice thickness. In summary, the observations show an interannual variability in ice thickness at higher frequency, and of greater amplitude, than simulated by regional Arctic models.

The mismatch between the observed variability and that predicted by models led us to investigate the origin of this variability. We compared the change in winter ice thickness with the length of intervening melt season, determined using satellite passive microwave radiometry[11] (Fig. 3b), by averaging all available data across the Arctic. Despite the fact that the spatial overlap between the two data sets is variable, we find a significant ($R^2 = 0.924$) correlation between the change in the altimeter-derived thickness between consecutive winters, and the melt season length during the intervening summer. Using a Monte Carlo simulation, we have calculated the change to the correlation that might occur if the altimeter estimates included thin ice and open water by adding a random component, with a standard deviation of 10 cm, to our average winter thickness estimates. Assuming a worst-case scenario, where the contribution of thin ice and open water to the change in mean winter ice thickness is uncorrelated with either the melt season length, or with the change in the altimeter thickness, the correlation is still significant ($R^2 = 0.745$). The regression implies that an increase in the melt season length by one day results in an extra 4.9 cm of summer ice melt. *In situ* measurements obtained during 1997 at one location in the Beaufort Sea suggest typical surface melt rates[30] of 1.7 ± 0.5 cm per day. The difference between these figures may be due to varying melt rates across the Arctic, or to related changes in bottom melt, which continues beyond surface freeze-up[30]. The observed dominant control of summer melt on the interannual variability of mean ice thickness (Fig. 3b) is in sharp contrast with the majority of models, which suggest that ice thickness variability in the Arctic Ocean is controlled mainly by wind and ocean forcing[6–8,10]. It had also been speculated[7,14] that reversal of the Arctic circulation in 1997 might lead to a thickening of the Arctic pack during the late 1990s. Instead, our data show a continued thinning of Arctic ice beyond 1998.

Our results show that errors are present in current simulations of Arctic sea ice, either in the radiative forcing, or in the parameterization of the effect of surface melt on the absorption of shortwave radiation. The observed variability of Arctic sea ice thickness, which shows that the sea ice mass can change by up to 16% within one year, contrasts with the concept of a slowly dwindling ice pack, produced by greenhouse warming[13]. This variability must be taken into account when determining the significance of trends derived from intermittent submarine measurements of ice draught. Although changes in Arctic circulation patterns may alter the distribution of ice thickness in the Arctic, we conclude that a continuation of the previously observed increase in melt season length[11] will lead to further overall thinning of Arctic sea ice. Until models properly reproduce the observed high-frequency, and thermodynamically driven, variability in sea ice thickness, simulations of both recent, and future, changes in Arctic ice cover will be open to question. □

Received 18 December 2002; accepted 10 September 2003; doi:10.1038/nature02050.

1. Carson, D. J. Climate modelling: Achievements and prospects. *Q. J. R. Meteorol. Soc.* **125,** 1–27 (1999).
2. Rind, D., Healy, R., Parkinson, C. & Martinson, D. The role of sea ice in $2 \times CO_2$ climate model sensitivity: Part II: hemispheric dependencies. *Geophys. Res. Lett.* **24,** 1491–1494 (1997).
3. Battisti, D. S., Bitz, C. M. & Moritz, R. E. Do general circulation models underestimate the natural variability in the Arctic climate? *J. Clim.* **10,** 1909–1920 (1997).
4. Houghton, J. T. *et al. Climate Change 2001: The Scientific Basis* (Cambridge Univ. Press, 2001).
5. Hilmer, M. & Lemke, P. On the decrease of Arctic sea ice volume. *Geophys. Res. Lett.* **27,** 3751–3754 (2000).
6. Polyakov, I. V. & Johnson, M. A. Arctic decadal and interdecadal variability. *Geophys. Res. Lett.* **27,** 4097–4100 (2000).
7. Zhang, J. L., Rothrock, D. & Steele, M. Recent changes in Arctic sea ice: The interplay between ice dynamics and thermodynamics. *J. Clim.* **13,** 3099–3114 (2000).
8. Zhang, Y. X. & Hunke, E. C. Recent Arctic change simulated with a coupled ice-ocean model. *J. Geophys. Res.* **106,** 4369–4390 (2001).
9. Chapman, W. L., Welch, W. J., Bowman, K. P., Sacks, J. & Walsh, J. E. Arctic sea ice variability: Model sensitivities and a multidecadal simulation. *J. Geophys. Res.* **99,** 919–935 (1994).
10. Holloway, G. & Sou, T. Has Arctic sea ice rapidly thinned? *J. Clim.* **15,** 1691–1701 (2002).
11. Smith, D. M. Recent increase in the length of the melt season of perennial Arctic sea ice. *Geophys. Res. Lett.* **25,** 655–658 (1998).
12. Steele, M. & Flato, G. M. in *The Freshwater Budget of the Arctic Ocean* 549–587 (Kluwer Academic, Dordrecht, 2000).
13. Manabe, S., Stouffer, R. J., Spelman, M. J. & Bryan, K. Transient responses of a coupled ocean-atmosphere model to gradual changes of atmospheric CO_2. Part 1: Annual mean response. *J. Clim.* **4,** 785–818 (1991).
14. Rothrock, D., Zhang, J. & Yu, Y. The Arctic ice thickness anomaly of the 1990s: A consistent view from observations and models. *J. Geophys. Res.* **108,** doi:10.1029/2001JC001208 (2003).
15. Rothrock, D. A., Yu, Y. & Maykut, G. A. Thinning of the Arctic sea-ice cover. *Geophys. Res. Lett.* **26,** 3469–3472 (1999).
16. Wadhams, P. & Davis, N. R. Further evidence for ice thinning in the Arctic Ocean. *Geophys. Res. Lett.* **27,** 3973–3975 (2000).
17. Tucker, W. B., Weatherly, J. W., Eppler, D. T., Farmer, L. D. & Bentley, D. L. Evidence for rapid thinning of sea ice in the western Arctic Ocean at the end of the 1980s. *Geophys. Res. Lett.* **28,** 2851–2854 (2001).
18. Polyakov, I. V., Proshutinsky, A. Y. & Johnson, M. A. Seasonal cycles in two regimes of Arctic climate. *J. Geophys. Res.* **104,** 25761–25788 (1999).
19. Peacock, N. R. & Laxon, S. W. Sea surface height determination in the Arctic Ocean from ERS altimetry. *J. Geophys. Res.* (in the press).
20. Beaven, S. G. *et al.* Laboratory measurements of radar backscatter from bare and snow-covered saline ice sheets. *Int. J. Remote Sens.* **16,** 851–876 (1995).
21. Wadhams, P. *et al.* Relationship between sea ice freeboard and draft in the Arctic basin, and implications for ice thickness monitoring. *J. Geophys. Res.* **97,** 20325–20334 (1992).
22. Warren, S. G. *et al.* Snow depth on Arctic sea ice. *J. Clim.* **12,** 1814–1829 (1999).

23. Radionov, V. F., Bryazgin, N. N. & Aleksandrov, Y. I. *The Snow Cover of the Arctic Basin* (Gidrometeoizdat, St. Petersburg, 1996).
24. Babko, O., Rothrock, D. A. & Maykut, G. A. Role of rafting in the mechanical redistribution of sea ice thickness. *J. Geophys. Res.* **107,** doi:10.1029/1999JC000190 (2002).
25. Wadhams, P. & Horne, R. J. An analysis of ice profiles obtained by submarine sonar in the Beaufort sea. *J. Glaciol.* **25,** 401–424 (1980).
26. Lindsay, R. W. & Rothrock, D. A. Arctic sea ice leads from advanced very high resolution radiometer images. *J. Geophys. Res.* **100,** 4533–4544 (1995).
27. Bourke, R. H. & McLaren, A. S. Contour mapping of Arctic Basin ice draft and roughness parameters. *J. Geophys. Res.* **97,** 17715–17728 (1992).
28. Haas, C. & Eicken, H. Interannual variability of summer sea ice thickness in the Siberian and central Arctic under different atmospheric circulation regimes. *J. Geophys. Res.* **106,** 4449–4462 (2001).
29. Gregory, J. M. *et al.* Recent and future changes in Arctic sea ice simulated by the HadCM3 AOGCM. *Geophys. Res. Lett.* **29,** doi:10.1029/2001GL014575 (2002).
30. Eicken, H., Tucker, W. B. & Perovich, D. K. Indirect measurements of the mass balance of summer Arctic sea ice with an electromagnetic induction technique. *Ann. Glaciol.* **33,** 194–200 (2001).

Acknowledgements We thank the European Space Agency for the provision of ERS data, and the National Snow and Ice Data Centre for submarine and passive microwave data. We also thank J. Mansley for assistance with data processing, and D. Wingham for comments. This work was supported by the UK Natural Environment Research Council and the European Union.

Competing interests statement The authors declare that they have no competing financial interests.

Correspondence and requests for materials should be addressed to S.L. (swl@cpom.ucl.ac.uk).

Neuroanatomy of flying reptiles and implications for flight, posture and behaviour

Lawrence M. Witmer[1], Sankar Chatterjee[2], Jonathan Franzosa[3] & Timothy Rowe[3]

[1]*Department of Biomedical Sciences, College of Osteopathic Medicine, Ohio University, Athens, Ohio 45701, USA*
[2]*Museum of Texas Tech University, Box 43191, Lubbock, Texas 79409, USA*
[3]*Jackson School of Geosciences, University of Texas, Austin, Texas 78712, USA*

Comparison of birds and pterosaurs, the two archosaurian flyers, sheds light on adaptation to an aerial lifestyle. The neurological basis of control holds particular interest in that flight demands on sensory integration, equilibrium, and muscular coordination are acute[1–8]. Here we compare the brain and vestibular apparatus in two pterosaurs based on high-resolution computed tomographic (CT) scans from which we constructed digital endocasts. Although general neural organization resembles birds, pterosaurs had smaller brains relative to body mass than do birds. This difference probably has more to do with phylogeny than flight, in that birds evolved from nonavian theropods that had already established trends for greater encephalization[5,9]. Orientation of the osseous labyrinth relative to the long axis of the skull was different in these two pterosaur species, suggesting very different head postures and reflecting differing behaviours. Their enlarged semicircular canals reflect a highly refined organ of equilibrium, which is concordant with pterosaurs being visually based, aerial predators. Their enormous cerebellar floccular lobes may suggest neural integration of extensive sensory information from the wing, further enhancing eye- and neck-based reflex mechanisms for stabilizing gaze.

The first vertebrate fliers were pterosaurs, an exclusively Mesozoic group that most workers[10] regard as close relatives of Dinosauria within Archosauria (Fig. 1a). Pterosaurs were lightly built, and their fossils are rare and often badly crushed. Virtual endocasts derived from CT scans of nearly complete skulls of two pterosaurs (Fig. 1)—the more basal *Rhamphorhynchus* and the pterodactyloid *Anhanguera*—are the most complete to date (Fig. 2; see Methods

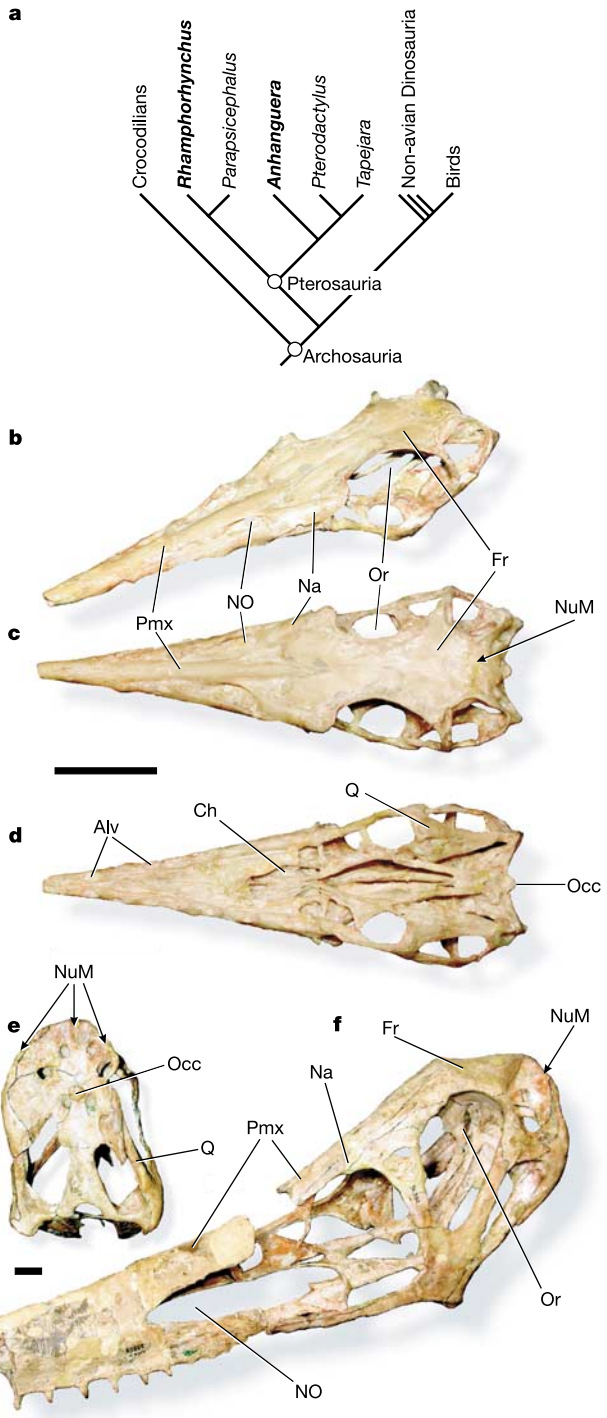

Figure 1 Relationships and skulls of pterosaur taxa. **a**, Cladogram of taxa mentioned in text and including pterosaurs for which endocast data are available. Topology based on ref. 19. **b–d**, *Rhamphorhynchus muensteri* (CM 11434, Jurassic, Germany) in left rostrodorsolateral (**b**), dorsal (**c**), and ventral (**d**) views. **e**, **f**, *Anhanguera santanae* (AMNH 25555, Cretaceous, Brazil) in caudal (**e**) and left rostrodorsolateral (**f**) views. Scale bar equals 20 mm. Alv, alveoli; Ch, choana; Fr, frontal; Na, nasal; NO, narial opening (confluent with antorbital fenestra in *Anhanguera*); NuM, area of attachment of nuchal (neck) musculature; Occ, occipital condyle; Or, orbit; Pmx, premaxilla; Q, quadrate.